Journal of Peptide Science
J. Peptide Sci. **6**: 550–559 (2000)

The Solution Structure of the *C*-terminal Segment of Tau Protein

G. ESPOSITO[a,*], P. VIGLINO[a], M. NOVAK[b,c] and A. CATTANEO[c,1]

[a] Dipartimento di Scienze e Tecnologie Biomediche, Università di Udine, 33100 Udine, Italy
[b] Institute of Neuroimmunology, Slovak Academy of Sciences, 84246 Bratislava, Slovakia
[c] Neuroscience Program, INFM Biophysics Unit, International School for Advanced Studies (SISSA), 34013 Trieste, Italy

Received 23 February 2000
Accepted 8 April 2000

Abstract: Pathological changes in the microtubule associated protein tau, leading to tau-containing filamentous lesions, are a major hallmark common to many types of human neurodegenerative diseases, including Alzheimer's disease (AD). No structural data are available which could rationalize the extensive conformational changes that occur when tau protein is converted to Alzheimer's paired helical filaments (PHF). The *C*-terminal portion of tau plays a crucial role in the aggregation of tau into PHF and in the truncation process that generates cytotoxic segments of tau. Therefore, we investigated the solution structure of the hydrophobic *C*-terminal segment 423–441 of tau protein (PQLATLADEVSASLAKQGL) by ^{1}H 2D NMR spectroscopy. The peptide displays the typical NMR evidence consistent with a α-helix geometry with a stabilizing C-capping motif. The reported data represent the first piece of structural information on an important portion of the molecule and can have implications towards the understanding of its pathophysiology. Copyright © 2000 European Peptide Society and John Wiley & Sons, Ltd.

Keywords: tau protein; α-helix conformation; NMR of peptides; Alzheimer's disease; NMR structure; helix capping; C-capping; protection from proteolysis

INTRODUCTION

Pathological changes in the microtubule-associated protein tau, leading to tau-containing filamentous lesions, are a major hallmark common to many types of human neurodegenerative diseases [1–4], including Alzheimer's disease (AD) and familial frontotemporal dementias and Parkinsonism (FTDP-17), collectively named 'tauopathies'. In AD, the neuropathological picture related to tau (neurofibrillary tangles, dystrophic neurites, neuritic component of senile plaque) is the main correlative factor with cognitive decline [5,6]. Over ten mutations in the tau gene have been identified in about 20 FTDP-17 families [7–9] establishing the relevance of tau pathology for neurodegenerative tauopathies, and proving that lesions of tau can lead directly to neurodegeneration [10,11]. Thus, mutations are only the latest addition to a number of abnormal post-translational changes that have been demonstrated to occur in tauopathies. These include abnormal hyperphosphorylation [12], ubiquitination [13], glycation [14], glycosylation [15] and aberrant proteolysis [16–19].

Tau is a highly hydrophilic fibrous protein with a very uneven distribution of hydrophobic fragments

Abbreviations: AD, Alzheimer's disease; DQF-COSY, double-quantum-filtered correlation spectroscopy; FTDP-17, familial frontotemporal dementias and Parkinsonism; HPLC, high pressure liquid chromatography; NMR, nuclear magnetic resonance; NOESY, nuclear Overhauser effect spectroscopy; pH*, uncorrected pH meter reading; PHFs, paired helical filaments; ROESY, rotating frame Overhauser effect spectroscopy; TAD, torsion angle dynamics; tau-C, segment 423–441 of tau protein; TFE, 2,2,2-trifluoroethanol; TOCSY, total correlation spectroscopy; 2D, two-dimension.

* Correspondence to: Dipartimento di Scienze e Tecnologie Biomediche, Università di Udine, P. le Kolbe 4, 33100 Udine, Italy; e-mail: gesposito@makek.dstb.uniud.it
[1] E-mail: cattaneo@sissa.it

Copyright © 2000 European Peptide Society and John Wiley & Sons, Ltd.

[20] and of phosphorylation sites [2,3] along its sequence. No structural data on tau are available so far, except for a low resolution trimeric model obtained from transmission electron microscopy and secondary structure assessment based on CD measurements and primary-sequence predictions [20]. The hydropathic index profile exhibits the highest density of positive values, i.e. hydrophobic character, in correspondence of the repeat regions and the *C*-terminal segment [20]. The *C*-terminal portion of tau plays a crucial role in the aggregation of tau into paired helical filaments (PHFs) [21] and in the truncation process that generates cytotoxic fragments [22,23]. One of the earliest cleavage events in the course of neuronal apoptosis may occur in correspondence of the *C*-terminal hydrophobic region [4]. For this reason the solution structure of the hydrophobic *C*-terminal segment 423–441 of tau protein has been investigated by ^{1}H 2D NMR spectroscopy at 500 MHz.

MATERIALS AND METHODS

The 19-residue peptide PQLATLADEVSASLAKQGL, corresponding to the *C*-terminal segment 423–441 of the human microtubule-associated tau protein, was purchased from Tecnogen (Caserta, Italy), from which synthetic details can be obtained upon request. The peptide, henceforth referred to as tau-C (segment 423–441 of tau protein), had been characterized by mass-spectrometry (TOF-MALDI $M + H^+ = 1914.7$ a.m.u. versus theoretical molecular weight = 1912.2 a.m.u.) and was pure to 99.0% as assessed by reverse-phase HPLC (column: Aquapore RP-18 100×2.1 mm ID; eluents: $A = H_2O$, 0.1% TFA, $B = CH_3CN$, 0.1% TFA; gradient (time/%B) = 0/5, 5/5, 30/60, 35/95, 40/95, 43/5; retention time = 25.3 min). The compound was used without further purification by dissolving 4.6 and 2.1 mg of lyophilized powder, respectively, in H_2O/D_2O, 94/6 by volume ([tau-C] = 4.8 m*M*) and in H_2O/TFE-d_3 (perdeuterated 2,2,2-trifluoroethanol), 50/50 by volume ([tau-C] = 2.2 m*M*).The uncorrected pH-meter reading, pH*, of the native aqueous solution was 2.9 and microliter additions of 1 *M* NaOH and HCl solutions were employed to adjust its value first to 4.5, and then to 3.7. No pH adjustments were performed on the TFE/water solution (apparent pH* 3.5). ^{1}H NMR measurements were performed at 298 K (and 278 K in water) on a Bruker AM 500 spectrometer operating at 500 MHz. 2D spectra were acquired typically with a sweep width of 6493.5 Hz in water and 5376.3 Hz in TFE/water over 2 K points in t_2 and 512 points in t_1, by using the time proportional phase incrementation method [24] to achieve quadrature detection in the indirect dimension. Scalar connectivities were monitored by double-quantum-filtered correlation spectroscopy (DQF-COSY) [25] and TOCSY [26] experiments. The latter type of experiments were typically run by an inverse-detected-like *z*-filtered implementation [27] with $\gamma B_2/2\pi$ of $\sim$11 kHz and t_m $\sim$50 ms. Dipolar connectivities were observed by NOESY [28] or ROESY [29] with t_m values ranging between 120 and 250 ms. The rotating frame experiments were performed with an effective $\gamma B_2/2\pi$ of $\sim$2.7 kHz obtained by *diluting* power deposition throughout t_m [30]. The solvent resonance was always suppressed by 1–1.5 s low-power irradiation. Data were processed with Felix software (MSI), with zero filling in both time domains (final matrix dimensions 2048×2048 real points), 70°/90°-shifted squared-sine-bell apodization, right shift in t_1 dimension by one point to remove baseline offsets (the proper delay had been introduced prior to t_m increments [31]) and 9th order polynomial baseline correction in t_2. The spectra were internally referenced on the resonance of dioxane in water (3.750 ppm), and organic solvent isotopic impurity in the water/TFE mixture (3.918 ppm), respectively. Restrained modelling was performed by using the program DYANA [32]. Six thousand torsion angle dynamics steps were performed with a simulated annealing procedure (1200 steps at high temperature followed by slow cooling down throughout the remaining 4800 steps) on each of the 1000 initially generated structures. Finally, 2000 conjugate gradient minimization steps were calculated to release steric clashes, torsion strains, etc. The structures were visualized by means of the software MOLMOL [33].

RESULTS

Resonance Assignment and Conformational Interpretation

The NMR spectra of tau-C were assigned by following the standard sequential assignment procedure [34]. Table 1 lists the chemical shifts values in both solvent systems that were employed. The peptide was first monitored in water at pH* 2.9, i.e. the value reached on solubilization. Only the sequential α_i-NH_{i+1} dipolar connectivities were observed under these conditions in the ROESY spectra (dipolar

Copyright © 2000 European Peptide Society and John Wiley & Sons, Ltd.

Table 1 ^{1}H NMR Chemical Shifts[a] of Tau-C (Tau-protein *C*-terminal Segment 423–441) at 298 K in Water/TFE, Apparent pH* 3.5 (Upper Rows, Roman), and Water, pH* 2.9 (Lower Rows, Italic), with H^{α} Chemical Shift Deviations ($\Delta\delta H^{\alpha}$) from Reported Limiting Values [35,36]

Residue	H^{N}	H^{α}	H^{β}	H^{γ}	H^{δ}	Others	$\Delta\delta H^{\alpha}$
Pro423		4.43	2.50	2.06	3.42		0.01
		4.40	*2.46*	*2.04*	*3.42*		*−0.02*
Gln424	8.71	4.49	2.07, 2.21	2.43		7.40, 6.70	0.13
	8.78	*4.39*	*2.01/2.08*	*2.38*		*7.57, 6.88*	*0.05*
Leu425	8.25	4.28	1.66	1.66	0.90/0.97		−0.07
	8.47	*4.35*	*1.62*	*1.63*	*0.88/0.93*		*0.01*
Ala426	8.03	4.25	1.46				−0.09
	8.43	*4.38*	*1.41*				*0.06*
Thr427	7.57	4.24	4.38	1.30			−0.11
	8.00	*4.31*	*4.23*	*1.21*			*−0.04*
Leu428	7.87	4.20	1.66, 1.80	1.66	0.90/0.94		−0.15
	8.18	*4.33*	*1.63*	*1.63*	*0.88/0.93*		*−0.01*
Ala429	8.18	4.03	1.46				−0.31
	8.24	*4.25*	*1.39*				*−0.07*
Asp430	8.10	4.46	3.19, 2.93				−0.17
	8.24	*4.66*	*2.92*				*0.02*
Glu431	8.08	4.15	2.35, 2.21	2.63, 2.48			−0.14
	8.15	*4.38*	*2.05/2.15*	*2.49*			*0.03*
Val432	8.77	3.66	2.14	0.95, 1.06			−0.47
	8.11	*4.09*	*2.12*	*0.96*			*−0.03*
Ser433	8.26	4.13	4.00/4.08				−0.36
	8.31	*4.40*	*3.87/3.92*				*−0.07*
Ala434	8.09	4.20	1.54				−0.14
	8.36	*4.32*	*1.44*				*0.00*
Ser435	8.00	4.25	3.99/4.17				−0.24
	8.17	*4.40*	*3.89*				*−0.07*
Leu436	8.26	4.16	1.49, 1.92	1.88	0.84/0.87		−0.19
	8.06	*4.40*	*1.66*	*1.66*	*0.88/0.93*		*0.06*
Ala437	8.04	4.22	1.54				−0.12
	8.09	*4.27*	*1.40*				*−0.05*
Lys438	7.90	4.18	2.01	1.58/1.66	1.75	3.02, 7.59	−0.14
	8.12	*4.28*	*1.80/1.89*	*1.47*	*1.70*	*3.01, 7.53*	*−0.04*
Gln439	7.70	4.38	2.13, 2.34	2.51, 2.44		7.21, 6.50	0.02
	8.26	*4.34*	*2.03/2.16*	*2.40*		*7.49, 6.85*	*0.00*
Gly440	7.98	3.87, 4.12					0.11
	8.36	*3.96*					*0.00*
Leu441	7.76	4.51	1.65	1.65	0.89/0.92		0.16
	8.06	*4.32*	*1.64*	*1.64*	*0.86/0.94*		*−0.02*

[a] In ppm with ± 0.01 ppm uncertainty. The chemical shifts of magnetically inequivalent diastereotopic pairs are reported with a separation slash only when their stereospecific assignment could not be obtained. The stereospecifically assigned resonances are ordered according to their identifier index, i.e. $\beta 2$ $\beta 3$, $\gamma 2$, $\gamma 3$, etc., for methylene hydrogens, $\gamma 1$, $\gamma 2$, $\delta 1$, $\delta 2$, etc., for methyl groups. The additional chemical shifts (column 'Others') refer to $H^{\varepsilon 21}$, $H^{\varepsilon 22}$ (Gln424 and Gln439), and $H^{\varepsilon 2/\varepsilon 3}$ and H^{ζ} (Lys438). For Gly440, the $H^{\alpha 2}$ and $H^{\alpha 3}$ assignments are tentative (see text) and the $\Delta\delta H^{\alpha}$ value is given only for the first resonance, i.e. the *pro*R $C^{\alpha}H$ occurring in L-amino acids.

Copyright © 2000 European Peptide Society and John Wiley & Sons, Ltd.

connectivities were stronger in the rotating frame than in the laboratory frame). Similar results were also obtained when the temperature was lowered to 278 K. These findings, coupled to the absence of significant deviations of the CH chemical shifts from the limiting values observed for unstructured oligopeptides in water [35] (Table 1), feature the typical pattern of statistically random conformations. This inference was also confirmed after varying the pH*. Actually, as soon as pH* was raised to around 4, extensive precipitation occurred and the NMR spectra obtained under these conditions showed only the chemical shift changes determined by the titration of Asp430 and Glu431 side chains along with a sharp decrease in the signal-to-noise ratio due to poor solubility of tau-C at pH* ≥ 4. It is concluded that the isolated tau-C segment does not adopt any preferential secondary structure in water.

By contrast, in the TFE/water mixture, the dipolar connectivity network was much denser than that observed in pure water. The sequential-correlation linking relied essentially on NH_i-NH_{i+1} and β_i-NH_{i+1} contacts. The upfield deviation of the CH chemical shifts with respect to the limiting random-coil values [35,36] was continuous along the segment Leu425-Lys438 ($\langle \Delta\delta \rangle \cong -0.20 \pm 0.11$ ppm, Table 1). This finding, along with the observation, along the same segment, of a virtually uniform series of $J^3_{HNH^\alpha} \leq 6$ Hz, of the mentioned sequential NOEs and of the (α_i-$\beta_i + 3$ correlations (Figure 1), leads us to conclude that in TFE/water tau-C folds into a regular α-helix geometry extending from Ala426 up to Gln439. The additional medium-range class of contacts expected for an α-helix, i.e. the α_i-NH_{i+3} connectivity, could be reliably measured only in two

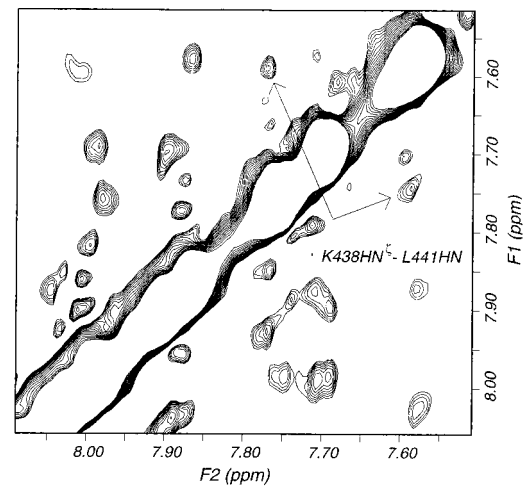

Figure 2 Section of the aromatic region of the ROESY spectrum of tau-C in TFE/water ($t = 120$ ms). The contour plot is drawn without distinction between positive and negative levels.

positions between the residue pairs 426–429 and 429–432 of the peptide) (Figure 1) because a unequivocal assessment was hampered by resonance overlap. On the other hand, the other α-helix-diagnostic contact, i.e. the α_i-NH_{i+4} connectivity, originates from the interaction between two hydrogens with canonical separation of 0.44 nm [34] which is close to the detectability threshold of dipolar interactions. In small molecules insufficiently slow tumbling rates and/or limited local fluctuations may adversely affect its observation. Interestingly, the only α_i-NH_{i+4} connectivity was detected between Ala437 and Leu441. In addition, Leu441 H^N

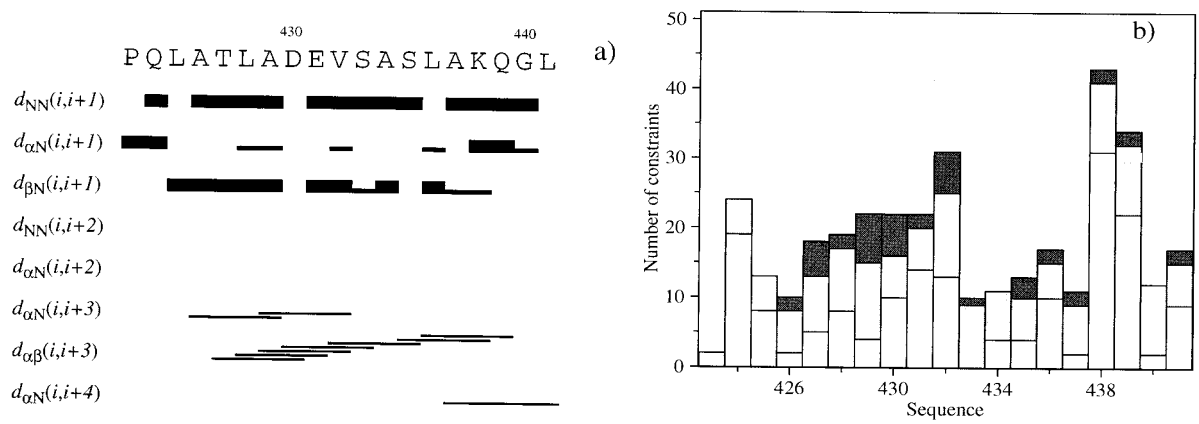

Figure 1 (a) Histogram of secondary-structure-diagnostic NOEs of tau-C in TFE/water. Bar heights are proportional to the experimental intensities of the corresponding connectivities. (b) Distribution of the observed NOE restraints along the sequence of tau C. Empty bars: intraresidue; pale-grey bars: sequential; dark-grey bars: medium range ($1 < |i-j| \leq 4$).

Copyright © 2000 European Peptide Society and John Wiley & Sons, Ltd.

exhibited a weak NOE also with Lys438 N^{ζ} hydrogens (Figure 2). The presence of these contacts, together with the magnetic inequivalence of the Gly440 C^{α} hydrogens, suggests a rigid geometry for Gly440 and Leu441, blocked onto the preceding helical region. In other words, the typical fraying pattern, commonly encountered at helix termini, is observed only at the three *N*-terminal residues of tau-C and not at the *C*-terminal amino acids. This result may indicate that the α-helix folding of tau-C is stabilized by a C-capping motif. The high occurrence frequency of Gly residues at helix *C*-termini is strongly correlated with their involvement in such motifs [37–39]. To assess whether this is the case also with tau-C, quantitative consistency must be found between the available set of conformational restraints and the molecular model.

Conformational Restraint Collection and Molecular Modelling

Dipolar connectivities were quantitated only in ROESY and NOESY spectra obtained in TFE/water. Following cross-peak sampling and integration, the obtained volumes were calibrated on the Asp430 $H^{\beta 2}$-$H^{\beta 3}$ geminal cross-peak, with an imposed separation value of 0.17 nm. The internuclear distances were calculated from single ROESY ($t_m = 120$ ms) and NOESY ($t_m = 150 \pm 10$ ms) spectra with upper and lower extrema of 0.50 and 0.17 nm, respectively. The calculated values were released by 10% and 20% to define lower and upper distance bounds, respectively, for isolated and nearly isolated cross peaks (overlap $\leq 10\%$). A larger allowance (20 and 40% for lower and upper bounds, respectively) was imposed for moderately overlapping connectivities (overlap $\leq 50\%$). Beyond 50% overlap, the connectivities were not taken into account for distance evaluation. Pseudoatom corrections [40] were applied for groups of equivalent nuclei and unidentified diastereotopic atoms or groups, a procedure that often leads to retain only a single distance bound because the other is meaninglessly short or long. Overall, 261 meaningful restraints could be collected, 135 upper limits and 126 lower limits (Figure 1), which were complemented with 34 torsion-angle range restraints. The latter were mostly φ and ψ angles, with uncertainty of $\pm 40°$ around the right-handed helix values, obtained by assessment of local secondary structure from the set of $J^3_{HNH^{\alpha}}$ coupling constants and dipolar connectivities. Only five χ^1 and one χ^2 dihedral angles, i.e. those of residues 424, 427, 430, 436, 439 and 431, respectively, were restrained, with an allowance of $\pm 50°$ around the limiting staggered values obtained through consideration of the local NOE pattern and the intervening coupling constants ($J^3_{H^{\alpha}H^{\beta}}$, $J^3_{H^{\beta}H^{\gamma}}$). Torsion-angle restraints were not imposed when the overall evidence was not complete in every feature. In a few instances, however, this incomplete evidence was qualitatively sufficient for stereospecific assignments. To some extent, this was also the case with Gly440. The $H^{\alpha 2}$ and $H^{\alpha 3}$ intraresidue NOEs to H^N did not match the qualitative estimate of the $J^3_{HNH^{\alpha}}$ values, whereas the sequential connectivities of the same pair to Leu441 H^N (essential for diastereotopic identification) gave conflicting results in ROESY and NOESY spectra. These incongruities are to be ascribed to the occurrence of the upfield Gly440 H^{α} resonance close to the TFE signal, leading to different extents of baseline deviations along either frequency axes in both spectra. Based on the more reliable evidence coming from the estimate of the $J^3_{HNH^{\alpha}}$ values, two conformational arrangements could be inferred for Gly440, i.e. α_L-helix like or α_R-helix like, depending on the stereospecific labelling given to the H^{α} resonances [41]. The modelling calculation results showed that the stereospecific assignment consistent with an α_L-helix-like geometry of Gly440 (see Tables 1 and 2) quantitatively fits better with the whole set of experimental restraints. Restrained modelling was performed by running molecular dynamics simulations based on the torsion angle dynamics (TAD) approach as implemented in the DYANA package [32]. Out of 1000 tau-C random conformers undergone to TAD, the 20 best fitting structures, i.e. those with the lowest global deviation from the input restraints (summarized by the target function parameter) were sorted out and submitted to statistical analysis. The low values of the average target function ($0.14 \pm 4.9 \times 10^{-3}$) and other average parameters, such as number of violations (0.0 ± 0.0), maximum violations ($0.11 \pm 0.01 \times 10^{-1}$ nm), sum of violations ($1.2 \pm 0.09 \times 10^{-1}$ nm), are the quantitative expression of the limited conformational spread within the selected structure family. The quality of the structural definition can be visually appreciated in Figure 3, showing the backbone best-fit superposition of the twenty conformers. As readily seen in Figure 3, the restrained molecular dynamics results confirm that the *C*-terminal end of tau-C is well defined, at variance with the geometry of the *N*-terminal end that exhibits a typical fraying pattern. Overall, the secondary structure of tau-C in TFE/water is an α_R

Copyright © 2000 European Peptide Society and John Wiley & Sons, Ltd.

Table 2 Structure Quality Parameters and Average Backbone Torsion Angles of Tau-C (Tau-protein C-terminal Segment 423–441) from DYANA Restrained Modelling Calculations

Structure statistics		
Parameter	Value	
Number of structures	20	
Average pairwise RMSD (segment 426–441)		
Backbone (/10^{-1} nm)	0.33 ± 0.15	(0.62–0.03)
Heavy atoms (/10^{-1} nm)	0.84 ± 0.29	(1.38–0.22)
Average RMSD from mean structure (segment 426–441)		
Backbone (/10^{-1} nm)	0.23 ± 0.09	(0.45–0.16)
Heavy atoms (/10^{-1} nm)	0.60 ± 0.20	(1.03–0.45)

Backbone torsion angles and dispersion parameters

Residue	φ	ξ [a]	ψ	ξ [a]
Pro423	–	–	60	0.45
Gln424	−88	1.00	69	1.00
Leu425	−117	1.00	163	0.50
Ala426	−52	1.00	−47	0.99
Thr427	−39	1.00	−61	0.99
Leu428	−43	0.98	−57	1.00
Ala429	−54	1.00	−47	0.99
Asp430	−57	0.99	−56	1.00
Glu431	−55	1.00	−36	1.00
Val432	−75	1.00	−39	1.00
Ser433	−51	1.00	−30	1.00
Ala434	−77	1.00	−55	1.00
Ser435	−41	1.00	−59	1.00
Leu436	−52	1.00	−37	1.00
Ala438	−70	1.00	−48	1.00
Lys439	−67	1.00	−10	1.00
Gly440	115	1.00	59	1.00
Leu441	−4	0.41	−12	0.71

[a] For any torsion angle of an ith residue, the dispersion parameter, ξ_i is defined as:

$$\xi_i = \frac{\langle \cos \theta_i \rangle}{\cos \alpha_i^{\theta}} = \frac{\langle \sin \theta_i \rangle}{\sin \alpha_i^{\theta}},$$

with

$$\alpha_i^{\theta} = \arctan \frac{\langle \cos \theta_i \rangle}{\langle \sin \theta_i \rangle} \pm \pi;\ \langle \cos \theta_i \rangle = \frac{1}{n} \sum_i \cos \theta_i;\ \langle \sin \theta_i \rangle = \frac{1}{n} \sum_i \sin \theta_i;\ \theta_i = \varphi, \psi, \chi^1, \text{etc.}$$

and n = number of structures.

helix spanning the segment 426–439, with conformational requirements for canonical H-bonds (NH_i-CO_{i-4} with i ranging from 430 to 438 except for $i = 435$, and NH_i-CO_{i-3} between Gln439 and Leu436) that are fulfilled in all or most of the 20 final structures. Further stabilization arises from the helix C-capping motif involving Gly440 and Leu441. The capping is made possible by the relative torsional freedom of the Gly residue that can adopt an α_L-like arrangement which allows extending the intramolecular H-bond network up to Leu441 H^N. The conformation of the last two residues of tau-C closely resembles the pattern reported for the Gly-based helix-C-capping motif

Copyright © 2000 European Peptide Society and John Wiley & Sons, Ltd.

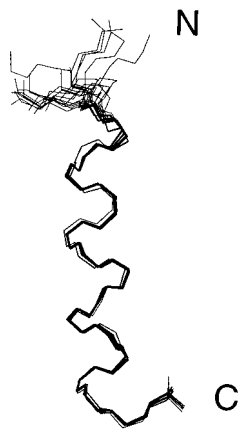

Figure 3 Backbone best-fit superposition for the lowest-target-function subset of 20 tau-C conformers resulting from NMR-restrained molecular dynamics calculations with DYANA [32].

known as Schellman motif [38,39]. Differently from the latter, however, the geometric conditions required for a bifurcated H-bond joining the amide hydrogens of residues 440 and 441 to the carbonyl of Ala437 occur consistently in all 20 structures (Figure 4). A canonical Schellman motif would have entailed the $H^N\cdots CO$ H-bonds 440–437 and 441–436 and hydrophobic interactions between side chains of Leu441 and Leu436. The lack of evidence in favour of the latter interactions (from our data, Leu441 side chain appears rather flexible) suggests that their absence is probably responsible for the deviation from the canonical pattern. Finally, additional H-bond-favourable geometry is also observed in all structures for Leu425 H^N and Pro423 CO (γ-turn-like [42] arrangement).

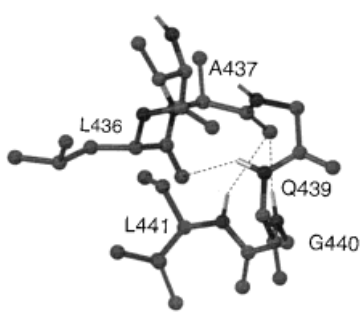

Figure 4 Helix C-capping motif of tau-C as obtained from NMR-restrained DYANA calculations. The motif, depicted for a single structure for sake of clarity, is consistently conserved within the final subset of 20 conformers. Side-chain heavy atoms are shown only for Leu436, Ala437 and Leu441.

DISCUSSION

In AD brains aberrant proteolysis of tau occurs [16–18] and truncated forms of tau, lacking their *C*-terminal portion, colocalize with DNA fragmentation, a marker for cell death [19]. In vitro, fragments of tau lacking the *C*-terminal portion induce cell death by apoptosis [22]. Conversely, in a culture model of neuronal apoptosis the production of tau fragments was found to be an early reversible event, with caspase-3 and calpain identified as proteases contributing to tau cleavage [23]. Interestingly, a caspase-3 cleavage site is located in the *C*-terminal end of tau (residue 421).

On the other hand, the accumulation of tau-containing aggregates accompanies diverse neurodegenerative diseases, collectively named tauopathies [43] and the *C*-terminal portion of tau has been shown to play a crucial role for the aggregation into PHFs [21,44–48].

Although the relation between tau aggregation and its apoptotic properties is currently unclear, these observations highlight the importance of the *C*-terminal portion of the molecule in determining its pathological properties. This led us to investigate the solution structure of the hydrophobic *C*-terminal segment 423–441 of tau protein, tau-C, by ^{1}H 2D NMR spectroscopy. Tau-C is sparingly soluble in water at pH* ≥ 4. At lower pH*, tau-C does not adopt any preferential secondary structure in water because of the overwhelming free energy contribution from solvent interactions with isolated oligopeptides. Resorting to aqueous–organic solvent mixtures, such as TFE/water, to overcome this free energy barrier is a common practice in structural studies of peptides, in order to highlight the structural propensities encoded by their primary sequence [49]. By following this approach, the previously predicted α-helix tendency of tau-C [20] is indeed observed. In addition, a further and unexpected helix stabilization element is observed, namely a C-capping motif due to the torsional freedom of Gly440 that can adopt an α_L-like arrangement which allows extending the intramolecular H-bond network up to Leu441 H^N. It might be argued that the occurrence of the latter structural element could be artifactual, i.e. due to the presence of the organic solvent. Capping motifs of isolated helices in TFE/water, however, appear to fit the same patterns obtained from statistical analyses of protein structures, again the solvent conditions eliciting those intramolecular contacts which are encoded by the primary sequence [50,51].

Copyright © 2000 European Peptide Society and John Wiley & Sons, Ltd.

Actually, helical peptides exhibit most often typical fraying patterns at their ends also in TFE/water [52,53]. Hence, the secondary structure elements shown by tau-C in TFE/water can be considered as genuine conformational trends.

The stability of the *C*-terminal helix, enhanced by the C-capping motif, may play a role for the selection of the early truncation site of tau [22,23]. Proteolysis commonly occurs at exposed flexible residues fulfilling the specificity requirements of the protease [54]. Thus, an exposed frayed helix-C-end would hardly escape the processing by cellular carboxypeptidases, leading to progressive unwinding of the helix by upstream shift of the frayed terminus. By contrast, under the same exposure conditions, a blocked helix terminus should exhibit a similar resistance to proteolysis as a stable helix. Helix capping motifs have been extensively addressed by many investigators (reviewed in Reference [39]). Besides the structural aspects, all of the studies stress the thermodynamic stabilization that these motifs impart to the helix or their plausible role as structure nucleating elements in early folding events. To the best of our knowledge, the possible role of helix capping motifs in protection from proteolysis has not been previously suggested, although evidence in favour of this role are already present in the literature [55]. Hen egg white lysozyme has been reported to be cleaved between residues 97 and 98 by limited thermolysin proteolysis (6 h incubation at 313 K) in TFE/water mixtures, and between residues 24–25 and 37–38 on extending the incubation time (24 h) [55]. In water, under the same conditions, the protein was not cleaved due to its well-packed and rigid structure. The outcome of the TFE/water experiment was ascribed to the perturbation of the tertiary structure undergone by the molecule in the aqueous–organic solvent mixture. As confirmed also by NMR investigation [56], TFE/water mixtures inhibit long-range hydrophobic interactions which drive tertiary folding, while favouring short-range interactions that are responsible for local secondary geometry. Limited proteolysis should affect only exposed flexible residues, whereas stable secondary structure elements, such as rigid helices, should be preserved even in TFE/water, in spite of the substantial loss of tertiary packing. In the lysozyme molecule there are other locations that meet the (quite broad) specificity requirements of thermolysin and should become as accessible in TFE/water as the sites undergoing cleavage. For instance, one such location should be adjacent to the *C*-terminus of helix A, i.e. G16–LI7 (similar to the native conformation in water, helix A extends up to H15 also in TFE/water [56]). By looking at the H-bond pattern of the lysozyme crystal structure [57] it can be immediately seen that G16 and L17 form a classical C-capping motif (Schellman type) that appears conserved in TFE/water [56]. Therefore, it can be concluded that lysozyme is not cleaved at the exposed *C*-terminus of helix A because of the presence of a stable C-capping motif which prevents flexibility.

The data here described represent the first piece of structural information on an important portion of tau molecule and can have implications towards the understanding of its pathophysiology. The stability within the cellular environment of a C-capped helix geometry at the *C*-terminal segment of tau may influence the selection of the site of an initial proteolytic attack. In particular, the cleavage of tau at residue 421 by the apoptotic protease caspase-3 could make the protein more prone to further proteolysis, generating apoptotic fragments [22].

Acknowledgements

This work was supported by the financial contribution of SIRS srl, INFM (sect. B) and DSTB. GE thanks Dr A. Makek for the assistance.

REFERENCES

1. Braak H, Braak E. Evolution of neuronal changes in the course of Alzheimer's disease. *J. Neural Trans. Suppl.* 1998; **53**: 127–140.
2. Mandelkow EM, Mandelkow E. Tau in Alzheimer's disease. *Trends Cell Biol.* 1998; **8**: 425–427.
3. Iqbal K, Alonso AC, Gong CX, Khatoon S, Pei JJ, Wang JZ, Grundke-Iqbal I. Mechanisms of neurofibrillary degeneration and the formation of neurofibrillary tangles. *J. Neural Trans. Suppl.* 1998; **53**: 169–180.
4. Novak M, Ugolini G, Fasulo L, Visintin M, Ovecka M, Cattaneo A. Truncation of tau and neurodegeneration. In *Alzheimer's Disease and Related Disorders*, vol. 31, Iqbal K, Swaab DF, Winblad B, Wisniewski HM (eds). Wiley: New York, 1999; 281–292.
5. Blessed G, Tornlinson BE, Roth M. The association between qualitative measures of dementia and senile change in the cerebral grey matter of elderly subjects. *Br. J. Psychiatry*. 1969; **114**: 797–811.
6. Terry RD. The pathogenesis of Alzheimer disease: an alternative to the amyloid hypothesis. *Neuropathol. Exp. Neurol.* 1996; **55**: 1023–1025.
7. Hutton M, Lendon CL, Rizzu P, Baker M, Froelich S, Houlden H, Pickering-Brown S, Chakraverty S, Isaacs A, Grover A, Hackett J, Adamson J, Lincoln S, Dickson

Copyright © 2000 European Peptide Society and John Wiley & Sons, Ltd.

D, Davies P, Petersen RC, Stevens M, de Graaff E, Wauters E, van Baren J, Hillebrand M, Joosse M, Kwon JM, Nowotny P, Che LK, Norton J, Morris JC, Reed LA, Troianowski J, Basun H, Lannfelt L, Neystat M, Fahn S, Dark F, Tannenberg T, Dodd PR, Hayward N, Kwok JBJ, Schofield PR, Andradis A, Snowden J, Crauffird D, Neary D, Owen F, Oostra BA, Hardy J, Goate A, van Swieten J, Mann D, Lynch T, Heutink P. Association of missense and 5′-splice-site mutations in tau with the inherited dementia FTDP-17. *Nature* 1998; **393**: 702–705.

8. Poorkaj P, Bird TD, Wijsman E, Nemens E, Garruto RM, Anderson L, Andreadis A, Wiederholt WC, Raskind M, Schellenberg GD. Tau is a candidate gene for chromosome 17 frontotemporal dementia. *Ann. Neurol.* 1998; **43**: 815–825.
9. Spillantini MG, Murrell JR, Goedert M, Farlow MR, Klug A, Ghetti B. Mutation in the tau gene in familial multiple system tauopathy with presenile dementia. *Proc. Natl. Acad. Sci. USA* 1998; **95**: 7737–7741.
10. Clark LN, Poorkaj P, Wszolek Z, Geschwind DH, Nasreddine ZS, Miller B, Li D, Payami H, Awert F, Markopoulou K, Andreadis A, D'Souza I, Lee VM, Reed L, Trojanowski JQ, Zhukareva V, Bird T, Schellenberg G, Wilhelmsen KC. Pathogenic implications of mutations in the tau gene in pallido-ponto-nigral degeneration and related neurodegenerative disorders linked to chromosome 17. *Proc. Natl. Acad. Sci. USA* 1998; **95**: 13103–13107.
11. Goedert M, Crowther A, Spillantini MG. Tau mutations cause frontotemporal dementias. *Neuron* 1998; **21**: 955–958.
12. Grundke-Iqbal I, Iqbal K, Tung YC, Quinlan M, Wisniewski HM, Binder LI. Abnormal phosphorylation of the microtubule-associated protein tau in Alzheimer cytoskeletal pathology. *Proc. Natl. Acad. Sci. USA* 1986; **83**: 4913–4917.
13. Mori H, Kondo J, Ihara Y. Ubiquitin is a component of paired helical filaments in Alzheimer's disease. *Science* 1987; **235**: 1641–1644.
14. Ledesma MD, Bonay P, Colaco C, Avila J. Analysis of microtubule-associated protein tau glycation in paired helical filaments. *J. Biol. Chem.* 1994; **269**: 21614–21619.
15. Wang JZ, Grundke-Iqbal I, Iqbal K. Glycosylation of microtubule associated protein tau: an abnormal post-translational modification in Alzheimer's disease. *Nature Med.* 1996; **2**: 871–875.
16. Novak M, Jakes R, Edwards P, Milstei C, Wischik C. Difference between Alzheimer PHF-core tau and normal tau revealed by epitope analysis of mAbs 423 and 7.51. *Proc. Natl. Acad. Sci. USA* 1991; **88**: 5837–5841.
17. Novak M, Kabat J, Wischik CM. Molecular characterization of the minimal protease resistant tau unit of the Alzheimer's disease paired helical filament. *EMBO J.* 1993; **12**: 365–370.
18. Novak M. Truncated tau protein as a new marker for Alzheimer's disease. *Acta Virologica* 1994; **38**: 173–189.
19. Ugolini G, Cattaneo A, Novak M. Co-localization of truncated tau and DNA fragmentation in Alzheimer's disease neurones. *Neuroreport* 1997; **8**: 3709–3712.
20. Ruben GC, Iqbal K, Grundke-Iqbal I, Wisniewski RM, Ciardelli TL, Johnson JE. The microtubule-associated protein tau forms a triple-stranded left-hand helical polymer. *J. Biol. Chem.* 1991; **266**: 22019–22027.
21. Yanagawa H, Chung SH, Ogawa Y, Sato K, Shibata-Seki T, Masai J, Ishiguro K. Protein anatomy: C-tail region of human tau protein as a crucial structural element in Alzheimer's paired helical filament formation *in vitro*. *Biochemistry* 1998; **37**: 1979–1988.
22. Fasulo L, Visintin M, Novak M, Cattaneo A. Tau truncation in Alzheimer's disease: expression of a fragment encompassing PHF core tau induces apoptosis in COS cells. *Alzheimer's Reports* 1998; **1**: 25–32.
23. Canu N, Dus L, Barbato C, Ciotti MT, Brancolini C, Rinaldi AM, Novak M, Cattaneo A, Bradbury A, Calissano P. Tau cleavage and dephosphorylation in cerebellar granule neurons undergoing apoptosis. *J. Neurosci.* 1998; **18**: 7061–7074.
24. Marion D, Wüthrich K. Application of phase sensitive two-dimensional correlated spectroscopy (COSY) for measurements of proton–proton spin–spin coupling constants in proteins. *Biochem. Biophys. Res. Commun.* 1983; **113**: 967–974.
25. Piantini U, Sorensen OW, Ernst RR. Multiple quantum filters for elucidating NMR coupling coherence. *J. Am. Chem. Soc.* 1982; **104**: 6800–6801.
26. Braunschweiler L, Ernst RR. Coherence transfer by isotopic mixing: application to proton correlation spectroscopy. *J. Magn. Reson.* 1983; **53**: 521–528.
27. Esposito G, Gibbons WA, Bazzo R. Phase coherence and solvent suppression in rotating-frame correlation experiments in liquids. *J. Magn. Reson.* 1988; **80**: 523–527.
28. Jeener J, Meier BH, Bachmann P, Ernst RR. Investigation of exchange processes by two-dimensional NMR spectroscopy. *J. Chem. Phys.* 1979; **71**: 4546–4553.
29. Bothner-By AA, Stephens RL, Lee J, Warren CD, Jeanloz RW. Structure determination of a tetrasaccharide: transient nuclear Overhauser effects in the rotating frame. *J. Am. Chem. Soc.* 1984; **106**: 811–813.
30. Kessler H, Griesinger C, Kesserbaum. R, Wagner K, Ernst RR. Separation of crossrelaxation and J cross-peaks in 2D rotating-frame NMR spectroscopy. *J. Am. Chem. Soc.* 1987; **109**: 607–609.
31. Marion D, Bax A. Baseline correction of 2D FT NMR spectra using a simple linear prediction extrapolation of the time-domain data. *J. Magn. Reson.* 1989; **83**: 205–211.
32. Güntert P, Mumenthaler C, Wüthrich K. Torsion angle dynamics for NMR structure calculation with the new program DYANA. *J. Mol. Biol.* 1997; **273**: 283–298.

Copyright © 2000 European Peptide Society and John Wiley & Sons, Ltd.

33. Koradi R, Billeter M, Wüthrich K. MOLMOL, a program for display and analysis of macromolecular structure. *J. Mol. Graphics* 1996; **14**: 51–55.
34. Wüthrich K (ed). *NMR Spectroscopy of Proteins and Nucleic Acids*. Wiley: New York, 1986.
35. Wishart DS, Bigarn CG, Holm A, Hodges RS, Sykes BD. ^{1}H, ^{13}C and ^{15}N random coil chemical shifts of common amino acids. 1. Investigations of nearest-neighbor effects. *J. Biomol. NMR* 1995; **5**: 167–168.
36. Merutka G, Dyson HJ, Wright PE. 'Random coil' ^{1}H chemical shifts obtained as a function of temperature and trifluoroethanol concentration for the peptide series GGXGG. *J. Biomol. NMR* 1995; **5**: 14–24.
37. Richardson JS, Richardson DC. Amino acid preferences for specific locations at ends of helices. *Science* 1988; **240**: 1648–1652.
38. Schellman C. The alpha-L conformation at the ends of helices. In *Protein Folding*, Jaenicke R (ed). Elsevier/North Holland: New York, 1980; 61–63.
39. Aurora R, Rose GD. Helix capping. *Protein Sci.* 1998; **7**: 21–38.
40. Wüthrich K, Billeter M, Braun W. Pseudo-structures for the 20 common amino acids for use in studies of protein conformations by measurements of intramolecular proton–proton distance constraints with nuclear magnetic resonance. *J. Mol. Biol.* 1983; **169**: 949–961.
41. Esposito G, Carver JA, Boyd J, Campbell ID. A high resolution ^{1}H NMR study of the solution structure of alamethicin. *Biochemistry* 1987; **26**: 1043–1050.
42. Némethy G, Printz MP. The γ-turn, a possible folded conformation of the polypeptide chain. Comparison with the β-turn. *Macromolecules* 1972; **5**: 755–758.
43. Spillantini MG, Goedert M. Tau protein pathology in neurodegenerative diseases. *Trends Neurosci.* 1998; **21**: 428–433.
44. Montejo de Garcini E, Avila J. In vitro conditions for the self-polymerization of the microtubule-associated protein, tau factor. *J. Biochem.* 1987; **102**: 1415–1421.
45. Lichtenberg-Kraag B, Mandelkow EM. Isoforms of tau protein from mammalian brain and avian erythrocytes: structure, self-assembly, and elasticity. *J. Struct. Biol.* 1990; **105**: 46–53.
46. Crowther RA, Olesen OF, Smith MJ, Goedert M. Assembly of Alzheimer-like filaments from full-length tau protein. *FEBS Lett.* 1994; **337**: 135–138.
47. Goedert M, Jakes R, Spillantini MG, Hasegawa M, Smith MJ, Crowther RA. Assembly of microtubule-associated protein tau into Alzheimer-like filaments induced by sulphated glycosaminoglycans. *Nature* 1996; **383**: 550–553.
48. Wille H, Drewes G, Biernat J, Mandelkow EM, Mandelkow E. Alzheimer-like paired helical filaments and antiparallel dimers formed from microtubule-associated protein tau in vitro. *J. Cell Biol.* 1992; **118**: 573–584.
49. Qian H, Chan SI. Interactions between a helical residue and tertiary structures: helix propensities in small peptides and in native proteins. *J. Mol. Biol.* 1996; **261**: 279–288.
50. Jiménez MA, Muñoz V, Rico M, Serrano IJ. Helix stop and start signals in peptides and proteins. The capping box does not necessarily prevent helix elongation. *J. Mol. Biol.* 1994; **242**: 487–496.
51. Esposito G, Dhanapal B, Dumy P, Varma V, Mutter M, Bodenhausen G. Lysine as helix C-capping residue in a synthetic peptide. *Biopolymers* 1997; **41**: 27–35.
52. Esposito G, Fogolari F, Viglino P, Cattarinussi S, De Magistris MT, Chiappinelli L, Pessi A. Conformational stabilization of a short pertussis toxin by end group protection and by incorporation into a multiple antigen peptide (MAP). A CD and NMR study. *Eur. J. Biochem.* 1993; **217**: 171–187.
53. Carver JA, Esposito G, Viglino P, Fogolari F, Guichard G, Briand JP, Van Regenmortel MHV, Brown F, Mascagni P. Structural analogy between retro-inverso and parent peptides. Molecular basis for the biological activity of a retro-inverso analogue of the immunodominant fragment of VP1 coat protein from foot-and-mouth disease virus. *Biopolymers* 1997; **41**: 569–590.
54. Fontana A, Fassina G, Vita C, Dalzoppo D, Zamai M, Zambonin M. Correlation between sites of limited proteolysis and segmental mobility in thermolysin. *Biochemistry*. 1986; **25**: 1847–1851.
55. Polverino De Laureto P, De Filippis V, Scaramella E, Zambonin M, Fontana A. Limited proteolysis of lysozyme in trifluoroethanol. Isolation and characterization of a partially active enzyme derivative. *Eur. J. Biochem.* 1995; **230**: 779–787.
56. Buck M, Schwalbe H, Dobson CM. Characterization of conformational preferences in a partly folded protein by heteronuclear NMR spectroscopy: assignment and secondary structure analysis of hen egg-white lysozyme in trifluoroethanol. *Biochemistry* 1995; **34**: 13219–13232.
57. Imoto T, Johnson LN, North ACT, Phillips DC, Rupley JA. Vertebrate lysozymes. In *The Enzymes*, vol. 7, Boyer PD (ed). Academic Press: New York, 1972; 665–868.

Copyright © 2000 European Peptide Society and John Wiley & Sons, Ltd.